EEDF in the COMPASS open divertor during a detachment experiment

M. Dimitrova[1,2], Tsv. K. Popov[3], R. Dejarnac[1], M. Komm[1], J. Cavalier[1], J. Seidl[1], J. Krbec[1,4], J. Stöckel[1], V. Weinzettl[1], P. Hacek[1,5], R. Panek[1] and the COMPASS team

[1] *Institute of Plasma Physics, The Czech Academy of Sciences, Prague, Czech Republic*

[2] *Emil Djakov Institute of Electronics, Bulgarian Academy of Sciences, Sofia, Bulgaria*

[3] *Faculty of Physics, St. Kl. Ohridski University of Sofia, Sofia, Bulgaria*

[4] *Faculty of Nuclear Sciences and Physical Engineering, Czech Technical University in Prague, Prague, Czech Republic*

[5] *Faculty of Mathematics and Physics, Charles University, Prague, Czech Republic*

1. Introduction

The COMPASS tokamak is equipped with a poloidal array of 39 Langmuir probes (LP) embedded in the divertor tiles [1, 2]. This work presents the results from swept probe measurements in a D-shaped, L-mode discharge (shot #12836), with a constant toroidal magnetic field B_T = 1.15 T and a plasma current I_{pl} =160 kA. In order to reach detachment, the plasma density (indicated by the line-average electron density, n_e^{avr}) was ramped up during the discharge. The n_e^{avr} varied from 3 to 8×10^{19} m^{-3}. The current-voltage characteristics measured at different n_e^{avr} were processed using the first-derivative probe technique [3, 4] to retrieve the plasma potential and the electron energy distribution function (EEDF).

2. Experimental results

Fig. 1 shows the temporal evolution of n_e^{avr}, and the ion saturation current, I_{sat}, measured by probe LP#6. This probe is located in the inner divertor region at the radial position R = 0.415 m, which, in this particular magnetic configuration, corresponds to the first probe just outside the inner strike point given by the magnetic reconstruction. The data are processed at different times during the density ramp-up, marked by different colour lines, corresponding to different line-average electron densities n_e^{avr} = [4, 4.5, 5.8, 7, 7.5]$\times10^{19}$ m^{-3}.

Fig. 2 presents the poloidal profiles of the ion saturation current density, J_{sat}, for the five different n_e^{avr}. The positions of the strike points from the magnetic reconstruction are indicated by dashed lines. It is clearly seen that, in the inner divertor and around the two strike-points, the ion saturation current density, J_{sat}, increases during the first part of the density ramp and then starts decreasing for the rest of the discharge as n_e^{avr} is still increasing.

This is also clearly seen in Fig. 1, where the signal from probe LP#6 decreases after peaking at 1135 ms (red line) for $n_e^{avr} = 4.5\times10^{19}$ m^{-3}. This roll-over is not observed in the far outer divertor (R > 0.525 m), where J_{sat} continuously increases as n_e^{avr} increases during the entire discharge. In the private flux region (PFR), all J_{sat} signals are lower.

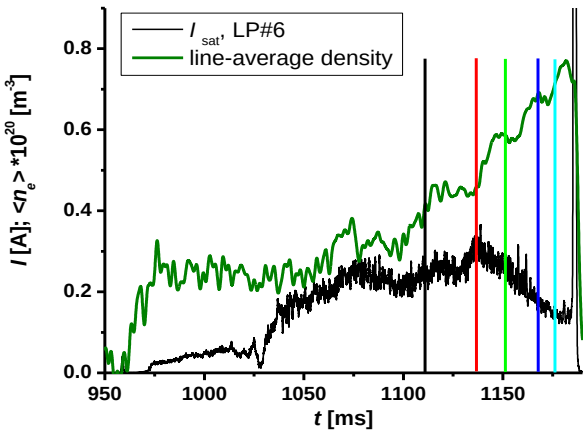

Fig. 1: Temporal profiles of the line-average electron density (green) and ion-saturation current of LP#6 (black) during discharge #12836.

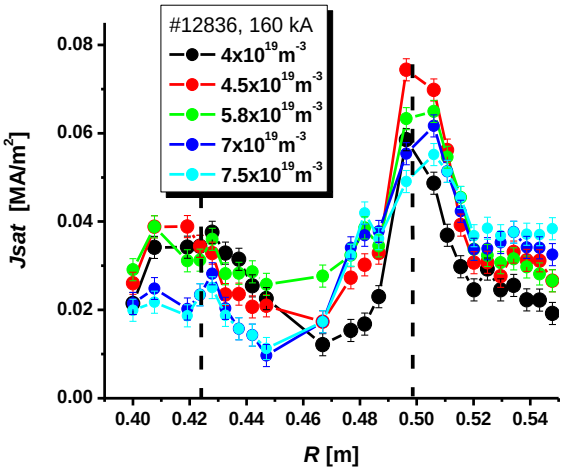

Fig. 2: Poloidal distribution of the ion saturation current density for different line-average densities during discharge #12836 in the COMPASS divertor.

The poloidal profiles of the floating, U_{fl}, and plasma, U_{pl}, potentials are shown in Fig. 3 a) and b), respectively. The magnitude of U_{fl} (Fig. 3 a) is larger for lower n_e^{avr}, with positive values at the inner divertor and in the PFR, and with negative values in the outer divertor. At high density, the U_{fl} profile is relatively flat with almost no peak at the strike-points.

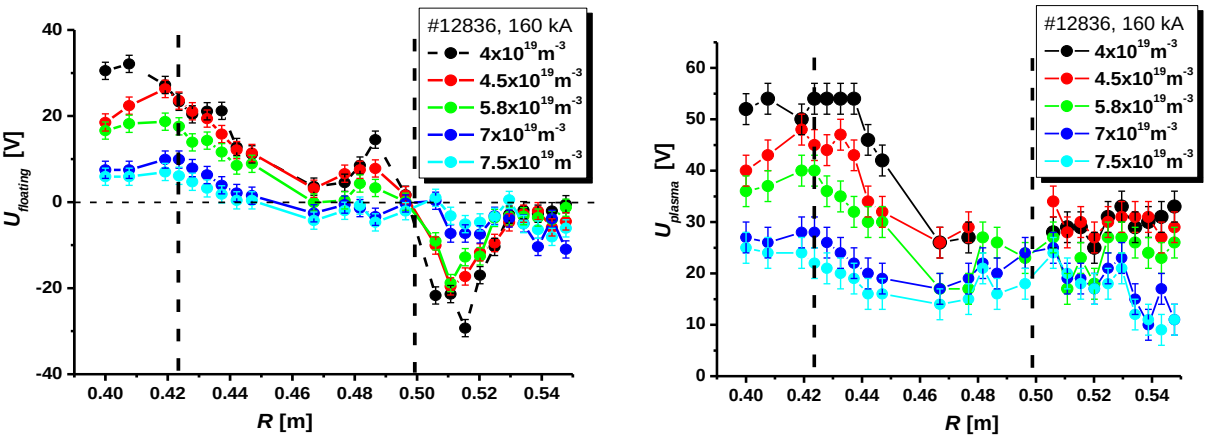

a) b)

Fig. 3: Poloidal distribution of **a)** the floating potential and **b)** the plasma potential for different line-average densities during discharge #12836 in the COMPASS divertor.

The plasma potential U_{pl} is positive in the entire divertor region (Fig. 3b). At the inner divertor, the plasma potential decreases with the increase in n_e^{avr}. This tendency is less pronounced in the outer divertor.

Fig. 4 a) presents the radial distributions of the electron temperatures in the divertor region versus the different n_e^{avr} considered. It is seen that during the discharge the EEDF changes from bi-Maxwellian to Maxwellian. At low values of n_e^{avr}, the EEDF is mainly bi-Maxwellian except in the far inner divertor region (R < 0.42 m) and in the middle of the PFR (0.46 < R < 0.48 m), where it is Maxwellian. The temperature of the low-energy group is in the range $T_e^l = 3.5 \pm 0.5$ eV (triangles), while the temperature of the high-energy group is in the range $T_e^h = (11 - 18) \pm 2$ eV (squares). The highest values are close to the outer strike point, for the lowest n_e^{avr}. When n_e^{avr} is increased to 5.8×10^{19} m^{-3}, the EEDF becomes Maxwellian in the inner divertor and in the PFR, while the EEDF in the outer divertor is still bi-Maxwellian. Above $n_e^{avr} = 7\times10^{19}$ m^{-3}, the EEDF is Maxwellian with a temperature 5 – 8 eV in the entire divertor region, which is the signature of a high recycling or partially detached divertor at high plasma density.

Fig. 4 b) presents the local electron density profiles for low $n_e^{avr} = 4\times10^{19}$ m^{-3}, when the EEDF is bi-Maxwellian; and for the high $n_e^{avr} = 7.5\times10^{19}$ m^{-3}, when the EEDF is Maxwellian. The low-temperature electron group (blue triangles) has a density higher than the high-temperature one (red squares).

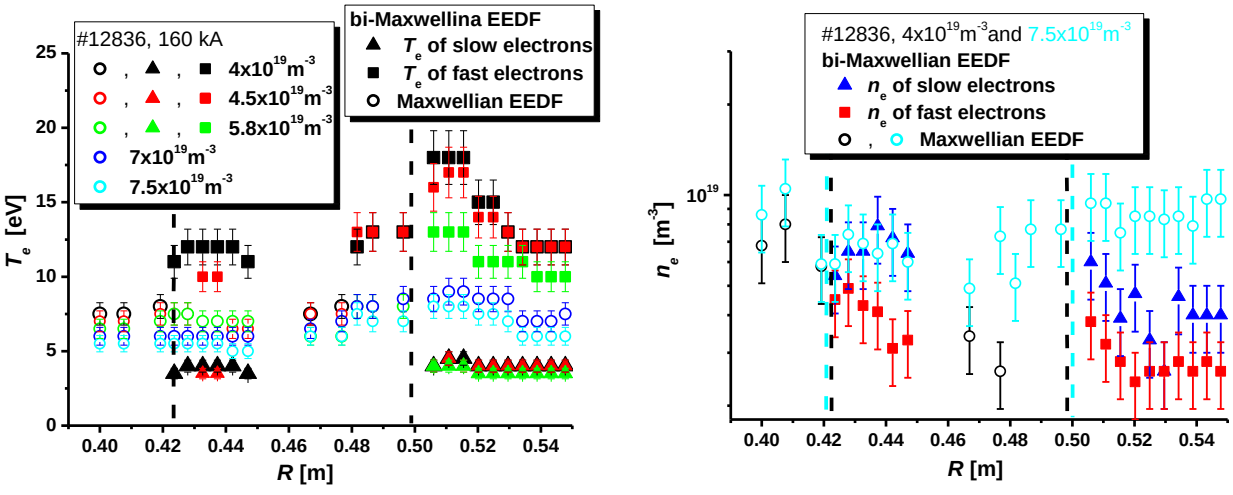

a) b)

Fig. 4: Poloidal distribution of **a)** the electron temperatures and **b)** the electron densities at different n_e^{avr} during discharge #12836 in the COMPASS divertor.

At $n_e^{avr} = 7\times10^{19}$ m^{-3}, when the EEDF is Maxwellian (turquoise empty circles), the local electron density around the inner strike-point is similar to the density of the low

temperature electron group at low n_e^{avr}, while at the outer divertor it exceeds significantly the densities of the low- and high-energy electron groups in the bi-Maxwellian case at low n_e^{avr}.

To explain the transition from bi-Maxwellian to Maxwellian EEDF, our proposition is as follows: The main cause for the bi-Maxwellian EEDF to arise is ionization of the neutrals by high-energy electrons, which are carried by the turbulent blobs crossing the separatrix from the confined plasma [3, 4]. At a high plasma density ($n_e^{avr} = 7.5\times10^{19}$ m^{-3}), along their path from the midplane to the divertor, the electrons relax and the EEDF is Maxwellian, while at a low plasma density ($n_e^{avr} = 4\times10^{19}$ m^{-3}), they can reach the divertor and the EEDF formed is bi-Maxwellian. This hypothesis is now under verification by massive parallel kinetic PIC simulations [5].

3. Summary

The paper presents the evolution of the EEDF and main plasma parameters in the COMPASS divertor when the plasma density increases (as indicated by the line-average electron density) in a L-mode discharge during the detachment campaign. The Langmuir probe measurements show that at the low line-average electron density of 4×10^{19} m^{-3}, the EEDF is bi-Maxwellian with a low-energy electron population with temperatures in the order of 4 eV (density in the range $2.5 – 8\times10^{18}$ m^{-3}) and a high-energy electron group with temperatures 11 – 18 eV (the density of this population being $2.5 – 5\times10^{18}$ m^{-3}). As the line-average electron density increases, the electron temperatures decrease. Above the line-average electron density of 7×10^{19} m^{-3}, the EEDF is found to be Maxwellian everywhere in the divertor with temperatures ranging from 5 eV to 8.5 eV and a local electron density in the range of 5.6×10^{18} m^{-3} – 1.2×10^{19} m^{-3}. A possible reason of the transition from a bi-Maxwellian to a Maxwellian EEDF is discussed.

Acknowledgements

This research has been partially supported by a Joint Research Project between the Institute of Plasma Physics of the CAS and the Institute of Electronics BAS BG, by the Czech Science Foundation grant GA16-24724S, by MSMT project # LM2015045 and by the Co-fund under MEYS project # 8D15001.

References

[1] R. Panek R et al.: Plasma Phys. Control. Fusion, Vol. 58 (2016), 014015.

[2] M. Dimitrova M, et al.: Contrib. Plasma Phys., Vol. 54, No. 3 (2014) 255 – 260.

[3] Tsv. K. Popov et al.: Plasma Phys. Control. Fusion, Vol. 57 (2015), 115011.

[4] Tsv. K. Popov et al.: Plasma Sources Sci. Technol., Vol. 25 (2016), 033001.

[5] D. Tskhakaya, Contrib. Plasma Phys., Vol. 52 (2012), 490 – 499.